Leveraging Radar Back-Scattered Data for Classification of Imaging Targets

Rahul Sharma*, Okan Yurduseven*,
*Institute of Electronics, Communication and Information Technology, Queen's University Belfast, UK, BT39DT,
rahul.sharma@qub.ac.uk

***Abstract*—Employing deep learning methodologies for computer vision tasks, particularly in the domain of radar image analysis, necessitates access to a large and diverse dataset. In the context of radar imagery, the creation of such a dataset often entails the intricate task of reconstructing images from raw radar back-scattered data. This reconstruction process involves handling substantial data volumes, which can be computationally intensve and time-consuming. In this research, a deep learning framework is proposed for target classification utilizing solely the radar back-scattered data, completely bypassing the need for image reconstruction procedure, thereby significantly reducing the classification time. To make the dataset generation easier, a computational imaging (CI) numerical model is employed. Subsequently, the deep learning model is trained using this dataset, and following the training phase, it is tested with radar back-scattered data that is not included in the network training. The outcomes of this evaluation confirm the benefit of training a deep learning model to perform image identification tasks based on radar back-scattered signatures.**

***Index Terms*—Deep learning, convolutional neural network, radar imaging, computational imaging**

I. Introduction

Deep learning techniques have shown remarkable success in addressing different computer vision tasks in context of radar imaging, such as classification [1], [2], object detection [3], [4], segmentation [5], [6], and image processing tasks, such as super-resolution [7], [8]. Leveraging these methodologies yields impressive results with rapid processing times. However, developing effective deep learning models for these tasks is not a straightforward task. It necessitates the generation of a substantial dataset for model training, and the lack of a universal model applicable across all tasks add to the complexity. Each specific task demands a tailored dataset of radar images for problem-solving. Generating such datasets for radar imagery is a multi-faceted process, involving the establishment of the imaging system, acquisition, processing of back-scattered data, and subsequent image reconstruction based on these measurements. This undertaking often involves the handling of large data volumes [9], particularly when dealing with electrically large imaging scenes, hence, making data generation for deep learning model development a formidable challenge.

This study presents a neural network architecture designed to directly analyze raw radar back-scattered measurements as input data and employ this information to classify the target responsible for generating the back-scattered data. This approach eliminates the need for time-consuming reconstruction and processing of images from the back-scattered measurements, streamlining the target classification process. The dataset generation for training the learning model is facilitated through the utilization of a computational imaging (CI) numerical model [10]. This model is specifically designed to simulate the acquisition of back-scattered data from diverse imaging targets. In the context of this study, the dataset is generated by employing two-dimensional (2D) computer-aided design (CAD) models representing a set of threat objects as the imaging targets. In essence, this research problem encompasses the classification of five distinct object classes.

II. Related Works

The integration of radar signals and deep learning models has gained significant attention in recent years. This section provides an overview of noteworthy contributions in this field. [11] showcased the substantial enhancement of automotive radar sensor classification capabilities through the application of deep learning methods. In [12], an innovative approach was introduced involving the fusion of millimetre-wave (mmW) radar and camera sensors using deep learning for object detection and tracking. [13] employed a convolutional neural network (CNN) to detect targets in radar data, primarily focusing on car detection within a 2D spatial context. [14] proposed a method for human identification based on radar micro-Doppler signatures, leveraging deep CNNs to extract discriminative features from these signatures, enabling accurate identification. In [15], results demonstrating the classification of diverse target classes in automotive radar systems was presented. their approach combined convolutional and recurrent neural network units for robust target classification. [16] also adopted a similar combination of convolutional and recurrent networks for the classification of moving targets. [17] proposed an innovative method for object detection type classification in automotive applications. This method harnessed deep learning techniques with radar reflections, providing valuable object class information for a diverse set of targets. Lastly, an efficient neural network classifier named EfficientNetv2-s was introduced for the classification and recognition of radar emitter signals, as detailed in [18].

These research efforts collectively illustrate the effective integration of radar signal processing and deep learning, showcasing its potential in diverse applications such as object detection and target classification in radar-based systems.

III. Data Generation

The set-up of the CI numerical model used for data generation is shown in Fig. 1.

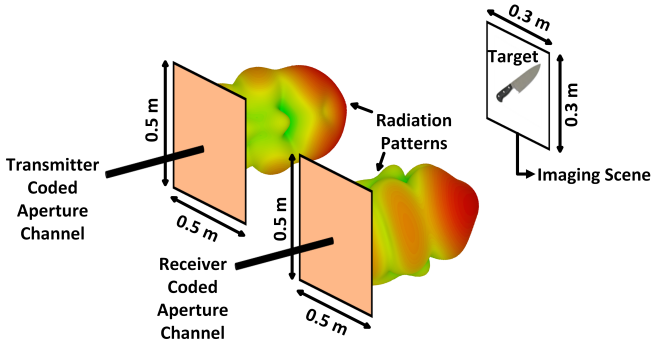

Fig. 1: The set-up of the imaging model used for data generation. The sizes of the transmit and receive coded apertures along with the imaging scene are highlighted.

As illustrated in Fig. 1, the numerical model incorporates two coded apertures [19], [20], one transmitter and one receiver, each measuring 0.5 m $\times$ 0.5 m ($\approx 30\lambda \times 30\lambda$), and separated by a distance of 0.0125 m. These coded apertures play a pivotal role in creating spatio-temporally varying radiation patterns for the purpose of probing the imaging scene. This method involves subjecting the transmitted and received electromagnetic waves to a sequence of diverse masks, each endowed with spatially dynamic transparency properties. To achieve this, a single mask is meticulously designed, featuring intricately distributed complex weights spanning its entire aperture [21]. This spatial-temporal transformation of the aperture enables the realization of a substantially enlarged aperture antenna capable of emitting quasi-random radiation patterns. One notable advantage of this technique lies in its ability to synthesize diverse measurement modes utilizing a single frequency. This synthesis empowers the generation of an array of radiation patterns, all meticulously designed to probe the imaging scene. This deliberate reconfiguration imparts a dynamic variation to the radiation field patterns from the antenna, ultimately enhancing the capabilities of the imaging system. For the studied CI model, the imaging scene, as specified in Fig. 1, has the dimension of 0.3 $\times$ 0.3 ($\approx 18\lambda \times 18\lambda$), and is located at a distance of 0.5 m from the transmitter and receiver apertures. The back-scattered from the imaging scene, depicted by $\mathbf{g}$, is modeled through the forward model expressed as:

$$\mathbf{g}_{M\times 1} = \mathbf{H}_{M\times N}\mathbf{f}_{N\times 1} + \mathbf{n}_{M\times 1} \tag{1}$$

Here, $\mathbf{H}$ denotes the sensing matrix, a fundamental element that correlates the recorded back-scattered measurements to the underlying imaging scene [22]. It is computed as the dot product of the transmit and receive electric fields across the entire measurements denoted by M measured for all N distinct pixels within the imaging scene. The scene's reflectivity distribution is characterized by the vector $\mathbf{f}$ and $\mathbf{n}$ denotes the measurement noise. It is modeled as additive Gaussian noise with zero-mean distribution. Its magnitude is governed by the signal-to-noise ratio (SNR) level, a key parameter that influences the performance and fidelity of the imaging system. Considering the resolution limit of the aperture, in this particular work, the imaging scene is discretized into N = 9,409 pixels, and number of measurements to acquire the scene information is equal to M = 500. The measurements are performed at a single frequency of 18 GHz, and the back-scattered measurements are subjected to a SNR level of 20 dB [23].

From the forward model equation outlined in (1), the generation of the back-scattered data, $\mathbf{g}$, is carried out for the development of the learning model. The dataset comprised of imaging targets classified into five distinct threat categories: guns, hammers, knives, scissors and wrenches. To this end, a total of 3,810 data points are generated, with the following distribution: 820 data points for guns, 800 for hammers, 980 for knives, 465 for scissors, and 750 for wrenches. To enhance the diversity and robustness of the dataset, these imaging targets are subjected to a series of geometric transformations. These transformations encompassed horizontal shifts both to the left and right, as well as vertical shifts to the top and bottom within the imaging scene. Moreover, flips along both the horizontal and vertical axes are introduced, adding further variability. This augmentation strategy substantially expanded the dataset to a total of 22,860 data points. For the subsequent stages, the dataset is partitioned, where 20,000 data points are reserved for the training phase, while the remaining 2,860 data points are selected for testing and evaluation of the model post-training. Fig. 2 presents an illustrative demonstration of the back-scattered data associated with two distinct imaging targets.

In Fig. 2(a) and (b), unique patterns of the back-scattered data that are specific to the respective target classes can be observed.

IV. Deep Learning Model

A. Model Architecture

In this section, details of the developed deep learning architecture for the classification problem are provided. The architecture is illustrated in Fig. 3.

As depicted in Fig. 3, the architectural framework consists of dual channels, each dedicated to processing distinct components of the input data: one channel for handling the real part and the other for managing the imaginary part. The specific filter sizes and quantities for the convolutional layers are specified in the figure. Within each channel, the architecture consists of a sequence of four layers, sequentially composed of convolutional operations, Rectified Linear Unit (ReLU) activation functions, and MaxPooling layers. Notably, at the second and fourth layers within each channel, dropout layers with a dropout rate of 0.5, is introduced, enhancing the model's robustness. Following this, the outputs from both channels are concatenated and subsequently flattened. The flattened

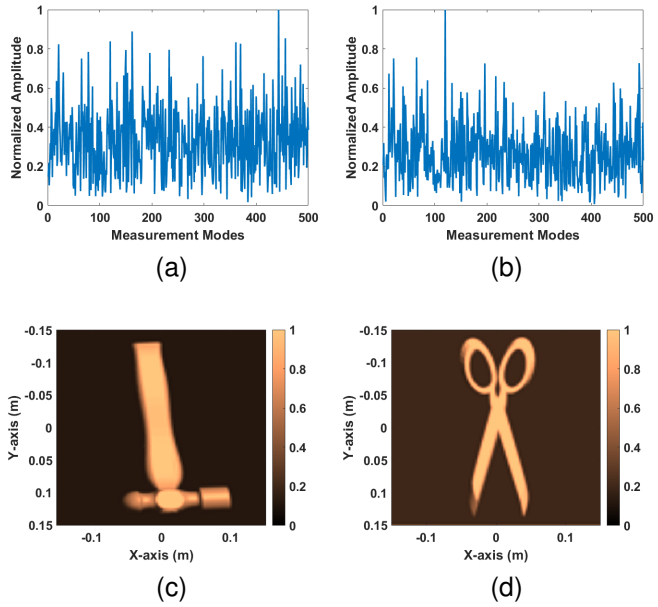

Fig. 2: (a) Absolute value of the back-scattered data gathered for target (c). (b) Absolute value of the back-scattered data gathered for target (d). The colourbars in (c) and (d) refer to the normalized reflectivity values.

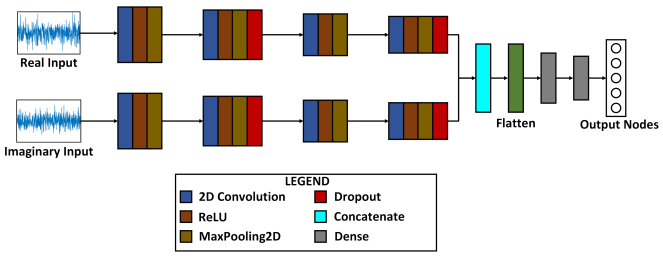

Fig. 3: The developed CNN architecture. The architecture uses two inputs - one dedicated for real part of the input data, and the other for imaginary part.

output is then directed through a densely connected neural network, featuring two layers with 512 and 128 neurons, respectively, for extracting high-level representations. Each of these dense layers is accompanied by a ReLU activation layer. Given that this specific problem entails five distinct classes, the architecture culminates in five output nodes, integrated with a softmax activation layer to output probabilistic class predictions.

B. Training Details

Upon finalizing the architecture of the deep learning model and completing the data generation process, the training phase is initiated. The training process is conducted using a NVIDIA GRID M60-8Q GPU equipped with 8 GB of dedicated RAM. The CNN model is implemented using TensorFlow and accelerated with CUDA platform. The learning rate used for training is 10^{-3} and the loss function used is sparse categorical cross-entropy loss [24], denoted by L_{SCC}, which is given by the formula:

$$L_{SCC} = -\frac{1}{N}\sum_{i=1}^{N}\sum_{j=1}^{C} y_{ij} log(p_{ij}) \tag{2}$$

where, N is the number of samples, C is the number of classes, y_{ij} is the indicator function that is 1 if the i-th sample belongs to the j-th class, and 0 otherwise. p_{ij} is the predicted probability of the i-th sample belonging to the j-th class. The choice of sparse categorical cross-entropy loss is motivated by the integer-encoded class labels used in this work (0, 1, 2, 3 and 4) for the five-class problem. The training process spanned a total of 500 epochs and employed the Adam optimizer for optimization [25]. The training and validation accuracy curves for the entire training process of 500 epochs are shown in Fig. 4.

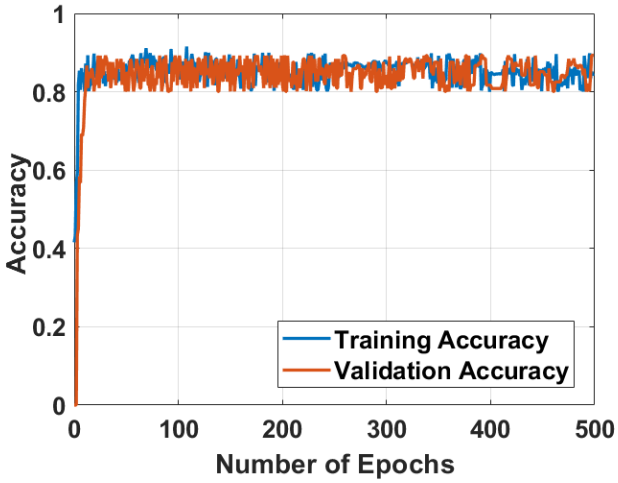

Fig. 4: Training and validation accuracy curves for 500 epochs.

V. Results and Discussion

The trained deep learning model is first tested on simulated radar data generated by the developed numerical model. As mentioned in Section III, out of the 22,860 data samples, 2,860 are reserved for testing the trained model. The confusion matrix and the classification report generated for the predictions during the testing phase of these simulated data samples are shown in Fig. 5 and Table I.

The precision, recall and F1-scores [26] for individual classes are detailed in Table I. Analyzing the results, it is evident that the model has demonstrated a high accuracy of 94% on the test dataset. Furthermore, the model's inference time for processing the entire dataset of 2,860 samples was recorded as 277.4 seconds, translating to a frame rate of 96.9 milliseconds per sample. This suggests that the proposed model can handle real-time scenarios.

The performance of the deep learning model is also assessed in the presence of noise, where back-scattered data generated by the numerical model is subjected to reduced SNR levels

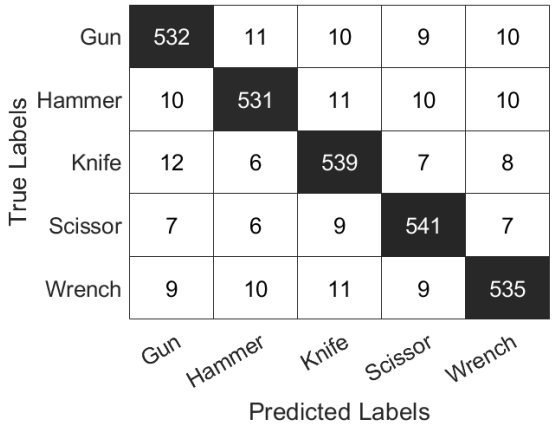

Fig. 5: Confusion matrix for 2,860 predictions.

Table I: Classification report for 2,860 predictions.

Class Name	Precision	Recall	F1-score	Support
Gun	0.93	0.93	0.93	572
Hammer	0.93	0.94	0.93	572
Knife	0.94	0.93	0.94	572
Scissor	0.95	0.94	0.94	570
Wrench	0.93	0.94	0.94	574
Accuracy			**0.94**	**2,860**
Macro-F1			**0.94**	**2,860**
Weighted-F1			**0.94**	**2,860**

of 10 dB and 5 dB. The model's accuracy is evaluated by feeding test data samples with SNR levels of 10 dB and 5 dB, respectively, into the learning model. The classification reports summarizing the model's performance under these conditions are presented in Tables II and III.

Table II: Classification report for test data samples of 10 dB SNR level.

Class Name	Precision	Recall	F1-score	Support
Gun	0.87	0.83	0.85	572
Hammer	0.85	0.86	0.85	572
Knife	0.84	0.83	0.84	572
Scissor	0.85	0.84	0.84	570
Wrench	0.84	0.88	0.86	574
Accuracy			**0.85**	**2,860**
Macro-F1			**0.85**	**2,860**
Weighted-F1			**0.85**	**2,860**

Tables II and III demonstrate a significant reduction in the model's accuracy, declining to 85% and 78%, respectively. This decline can be attributed to the elevated noise levels present in the back-scattered data. The model's training primarily focused on classifying targets using back-scattered data at a fixed SNR level of 20 dB, hence, consequently, the model exhibits reduced accuracy in handling data with lower SNR levels.

Table III: Classification report for test data samples of 5 dB SNR level.

Class Name	Precision	Recall	F1-score	Support
Gun	0.79	0.76	0.78	572
Hammer	0.76	0.77	0.77	572
Knife	0.78	0.77	0.78	572
Scissor	0.80	0.78	0.79	570
Wrench	0.75	0.79	0.77	574
Accuracy			**0.78**	**2,860**
Macro-F1			**0.78**	**2,860**
Weighted-F1			**0.78**	**2,860**

The classification accuracy on the dataset with elevated noise levels can be improved by modifying the model architecture through the incorporation of additional layers into the neural network. However, such modifications can lead to the development of a more complex network, resulting in an increased parameter count. Consequently, this may introduce overfitting issues during the training phase and subsequently prolong the inference time. Alternatively, another approach involves the adjustment of the training dataset by the inclusion of back-scattered data that has been subjected to SNR levels of 10 dB and 5 dB. Subsequently, the learning model is trained utilizing this revised dataset and evaluated on the test dataset. Detailed classification reports for the predictions post-training are included in Tables IV and V.

Table IV: Classification report for test data samples of 10 dB SNR level after training the model on new dataset.

Class Name	Precision	Recall	F1-score	Support
Gun	0.88	0.88	0.88	572
Hammer	0.89	0.88	0.89	572
Knife	0.88	0.89	0.89	572
Scissor	0.90	0.89	0.89	570
Wrench	0.89	0.89	0.89	574
Accuracy			**0.89**	**2,860**
Macro-F1			**0.89**	**2,860**
Weighted-F1			**0.89**	**2,860**

Table V: Classification report for test data samples of 5 dB SNR level after training the model on new dataset.

Class Name	Precision	Recall	F1-score	Support
Gun	0.84	0.85	0.85	572
Hammer	0.85	0.86	0.85	572
Knife	0.85	0.84	0.84	572
Scissor	0.86	0.84	0.85	570
Wrench	0.84	0.86	0.85	574
Accuracy			**0.85**	**2,860**
Macro-F1			**0.85**	**2,860**
Weighted-F1			**0.85**	**2,860**

As evident from the accuracy scores of 89% and 85% on test dataset subjected to 10 dB and 5 dB SNR levels, respectively,

it can be concluded that training the neural network with noisy data has resulted in a demonstrable improvement in the accuracy scores.

VI. Conclusion

In this work, an alternate approach to solve the classification problem in radar images leveraging deep learning model was presented. The proposed method does not rely on the reconstructed images from the radar imaging systems. Instead, the learning model was designed to predict the respective classes of the imaging target directly from the raw back-scattered data acquired during the radar imaging process. The data for the training and testing processes of the learning model were generated using a CI numerical model. The learning model was configured to accommodate the complex-valued back-scattered data, utilizing two separate channels for the real and imaginary components. Post training, the model was tested with 2,860 test samples, where the model achieved an accuracy score of 94% and an inference speed of 96.9 milliseconds per sample. Furthermore, the model was also tested on noisy dataset where the noise levels in the recorded back-scattered data were varied. The results demonstrated a noticeable decline classification accuracy to 85% and 78% at 10 dB and 5 dB SNR levels, respectively. A remedy to this issue was proposed in this work, wherein the training dataset was augmented with back-scattered data corresponding to higher noise levels. Following this adaptation, the model's classification accuracy significantly improved, reaching 89% at 10 dB SNR level and 85% at 5 dB SNR levels.

All these findings signify that the classification problem for targets can also be accurately solved, even in the presence of noise, by utilizing only the raw back-scattered data, thus, eliminating the need for the image reconstruction process. This can drastically simplify the signal processing layer of CI-based imaging systems offering significant potential for achieving real-time detection and classification.

Acknowledgment

This work was supported by the Leverhulme Trust under Research Leadership Award RL-2019-019.

References

[1] R. Sharma, R. Hussung, A. Keil, F. Friederich, T. Fromenteze, M. Khalily, B. Deka, V. Fusco, and O. Yurduseven, "Coded-aperture computational millimeter-wave image classifier using convolutional neural network," *IEEE Access*, vol. 9, pp. 119 830 – 119 844, Aug. 2021.

[2] X. Liu, Y. Wu, W. Liang, Y. Cao, and M. Li, "High resolution sar image classification using global-local network structure based on vision transformer and cnn," *IEEE Geoscience and Remote Sensing Letters*, vol. 19, pp. 1–5, 2022.

[3] A. Batra, M. Wiemeler, D. Göhringer, and T. Kaiser, "Geometrical shapes detection in high-resolution thz sar image," in *2022 19th European Radar Conference (EuRAD)*, 2022, pp. 1–4.

[4] Y. Gu, S. Meng, and K. Shi, "Radar-enhanced image fusion-based object detection for autonomous driving," in *2022 IEEE International Conference on Signal Processing, Communications and Computing (ICSPCC)*, 2022, pp. 1–6.

[5] M. A. Nuhoglu, Y. K. Alp, M. E. C. Ulusoy, and H. A. Cirpan, "Image segmentation for radar signal deinterleaving using deep learning," *IEEE Transactions on Aerospace and Electronic Systems*, vol. 59, no. 1, pp. 541–554, 2023.

[6] M. Hoffmann, T. Noegel, C. Schüßler, M. Vossiek, M. Schütz, and P. Gulden, "Filter-based segmentation of automotive sar images," in *2022 IEEE Radar Conference (RadarConf22)*, 2022, pp. 1–6.

[7] R. Sharma, J. Zhang, R. Kumar, B. Deka, V. Fusco, and O. Yurduseven, "3d super-resolution of coded aperture millimeter-wave images using complex-valued convolutional neural network," *IEEE Sensors Journal*, vol. 22, no. 21, pp. 20 921–20 936, Sep. 2022.

[8] C. Vasileiou, J. Smith, S. Thiagarajan, M. Nigh, Y. Makris, and M. Torlak, "Efficient cnn-based super resolution algorithms for mmwave mobile radar imaging," in *2022 IEEE International Conference on Image Processing (ICIP)*, 2022, pp. 3803–3807.

[9] O. Yurduseven, J. N. Gollub, A. Rose, D. L. Marks, and D. R. Smith, "Design and simulation of a frequency-diverse aperture for imaging of human-scale targets," *IEEE Access*, vol. 4, pp. 5436–5451, 2016.

[10] R. Sharma, O. Yurduseven, B. Deka, and V. Fusco, "Hardware enabled acceleration of near-field coded aperture radar physical model for millimetre-wave computational imaging," *Progress in Electromagnetic Research B*, vol. 90, pp. 91–108, Jan. 2021.

[11] K. Patel, K. Rambach, T. Visentin, D. Rusev, M. Pfeiffer, and B. Yang, "Deep learning-based object classification on automotive radar spectra," 07 2019.

[12] J.-J. Lin, J.-I. Guo, V. M. Shivanna, and S.-Y. Chang, "Deep learning derived object detection and tracking technology based on sensor fusion of millimeter-wave radar/video and its application on embedded systems," *Sensors*, vol. 23, no. 5, 2023. [Online]. Available: https://www.mdpi.com/1424-8220/23/5/2746

[13] M. Dreher, E. Erçelik, T. Bänziger, and A. Knoll, "Radar-based 2d car detection using deep neural networks," in *2020 IEEE 23rd International Conference on Intelligent Transportation Systems (ITSC)*, 2020, pp. 1–8.

[14] P. Cao, W. Xia, M. Ye, J. Zhang, and J. Zhou, "Radar-id: Human identification based on radar micro-doppler signatures using deep convolutional neural networks," *IET Radar, Sonar Navigation*, vol. 12, 03 2018.

[15] A. Angelov, A. Robertson, R. Murray-Smith, and F. Fioranelli, "Practical classification of different moving targets using automotive radar and deep neural networks," *IET Radar, Sonar Navigation*, vol. 12, 04 2018.

[16] S. Kim, S. Lee, S. Doo, and B. Shim, "Moving target classification in automotive radar systems using convolutional recurrent neural networks," pp. 1482–1486, 2018.

[17] M. Ulrich, C. Gläser, and F. Timm, "Deepreflecs: Deep learning for automotive object classification with radar reflections," pp. 1–6, 05 2021.

[18] Z. Sun, K. Li, Y. Zheng, X. Li, and Y. Mao, "Radar spectrum image classification based on deep learning," *Electronics*, vol. 12, no. 9, 2023. [Online]. Available: https://www.mdpi.com/2079-9292/12/9/2110

[19] M. L. Don, C. Fu, and G. R. Arce, "Compressive imaging via a rotating coded aperture," *Appl. Opt.*, vol. 56, no. 3, pp. B142–B153, Jan 2017. [Online]. Available: https://opg.optica.org/ao/abstract.cfm?URI=ao-56-3-B142

[20] C. Watts, D. Shrekenhamer, J. Montoya, G. Lipworth, J. Hunt, T. Sleasman, D. Smith, and W. Padilla, "Terahertz compressive imaging with metamaterial spatial light modulators," *Nature Photonics*, vol. 8, 08 2014.

[21] T. Sleasman, M. F. Imani, J. N. Gollub, and D. R. Smith, "Dynamic metamaterial aperture for microwave imaging," *Applied Physics Letters*, vol. 107, no. 20, 11 2015. [Online]. Available: https://www.osti.gov/biblio/22486109

[22] T. V. Hoang, V. Fusco, T. Fromenteze, and O. Yurduseven, "Computational polarimetric imaging using two-dimensional dynamic metasurface apertures," *IEEE Open Journal of Antennas and Propagation*, vol. 2, pp. 488–497, 2021.

[23] O. Yurduseven, M. Imani, H. Odabasi, J. Gollub, G. Lipworth, A. Rose, and D. Smith, "Resolution of the frequency diverse metamaterial aperture imager," *Progress in Electromagnetics Research*, vol. 150, pp. 97–107, 2015, publisher Copyright: © 2015, Electromagnetics Academy. All rights reserved.

[24] X. Chai, W. Nie, K. Lin, G. Tang, T. Yang, J. Yu, and W. Cao, "An open-source package for deep-learning-based seismic facies classification: Benchmarking experiments on the seg 2020 open data," *IEEE Transactions on Geoscience and Remote Sensing*, vol. 60, pp. 1–19, 2022.

[25] D. Kingma and J. Ba, "Adam: A method for stochastic optimization," *International Conference on Learning Representations*, 12 2014.

[26] A. Geron, *Hands-on Machine Learning with Scikit-Learn, Keras, and TensorFlow : concepts, tools, and techniques to build intelligent systems*, second edition. ed. Sebastopol, CA: O'Reilly, 2019 - 2019.